ACCOUNTS
of chemical research

NMR at Low and Ultralow Temperatures

ROBERT TYCKO*

Laboratory of Chemical Physics, National Institute of Diabetes and Digestive and Kidney Diseases, National Institutes of Health, Bethesda, Maryland 20892-0520, United States

RECEIVED ON DECEMBER 29, 2012

CONSPECTUS

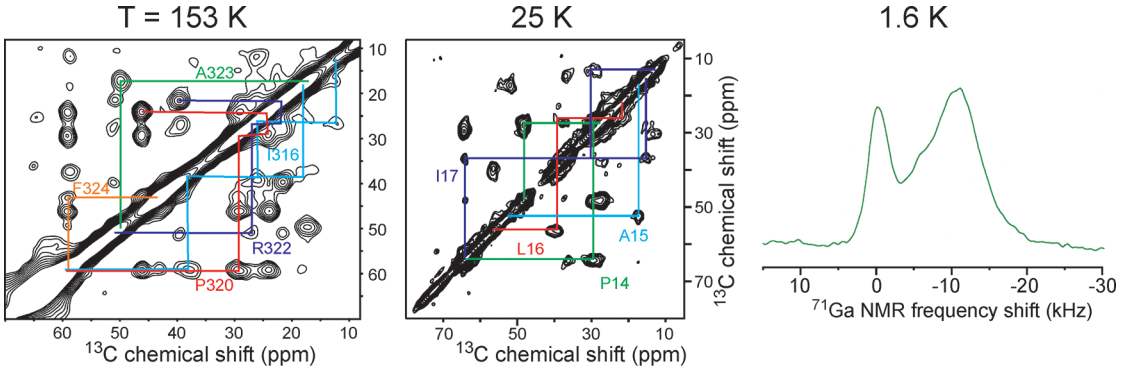

Solid state nuclear magnetic resonance (NMR) measurements at low temperatures have been common in physical sciences for many years and are becoming increasingly important in studies of biomolecular systems. This Account reviews a diverse set of projects from my laboratory, dating back to the early 1990s, that illustrate the motivations for low-temperature solid state NMR, the types of information that are available from the measurements, and likely directions for future research. These projects include NMR studies of both physical and biological systems, performed at low (cooled with nitrogen, down to 77 K) and ultralow (cooled with helium, below 77 K) temperatures, and performed with and without magic-angle spinning (MAS).

NMR studies of physical systems often focus on phenomena that occur only at low temperatures. Two examples from my laboratory are studies of molecular rotation and orientational ordering in solid C_{60} at low temperatures and studies of unusual electronic states, called skyrmions, in two-dimensionally confined electron systems within semiconductor quantum wells. To study quantum wells, we used optical pumping of nuclear spin polarizations to enhance their NMR signals. The optical pumping phenomenon exists only at ultralow temperatures.

In studies of biomolecular systems, low-temperature NMR has several motivations. In some cases, low temperatures suppress molecular tumbling, thereby permitting solid state NMR measurements on soluble proteins. Studies of AIDS-related peptide/antibody complexes illustrate this effect. In other cases, low temperatures suppress conformational exchange, thereby permitting quantitation of conformational distributions. Studies of chemically denatured states of the model protein HP35 illustrate this effect. Low temperatures and rapid freeze-quenching can also be used to trap transient intermediate states in a non-equilibrium kinetic process, as shown in studies of a transient intermediate in the rapid folding pathway of HP35.

NMR sensitivity generally increases with decreasing sample temperature. Therefore, it can be useful to carry out experiments at the lowest possible temperatures, particularly in studies of biomolecular systems in frozen solutions. However, solid state NMR studies of biomolecular systems generally require rapid MAS. A novel MAS NMR probe design that uses nitrogen gas for sample spinning and cold helium only for sample cooling allows a wide variety of solid state NMR measurements to be performed on biomolecular systems at 20–25 K, where signals are enhanced by factors of 12–15 relative to measurements at room temperature.

MAS NMR at ultralow temperatures also facilitates dynamic nuclear polarization (DNP), allowing sizeable additional signal enhancements and large absolute NMR signal amplitudes with relatively low microwave powers. Current research in my laboratory seeks to develop and exploit DNP-enhanced MAS NMR at ultralow temperatures, for example, in studies of transient intermediates in protein folding and aggregation processes and studies of peptide/protein complexes that can be prepared only at low concentrations.

Published on the Web 03/07/2013 www.pubs.acs.org/accounts
10.1021/ar300358z

Introduction

There are several motivations for performing nuclear magnetic resonance (NMR) measurements at low temperatures, including (1) to study phenomena that occur only at low temperatures; (2) to immobilize molecules in frozen solutions, thereby permitting solid state NMR measurements on soluble systems; (3) to trap transient states that would quickly disappear at higher temperatures; (4) to enhance the signal-to-noise of the NMR measurements; (5) to facilitate dynamic nuclear polarization and other hyperpolarization methods. This Account reviews research projects in my laboratory that have involved both low temperatures (defined as sample temperatures that can be achieved with liquid nitrogen) and ultralow temperatures (defined as sample temperatures that require liquid helium) and that illustrate these five motivations. Of course, many other laboratories have pursued low-temperature NMR measurements for various purposes and continue to do so. This Account does not include a review of work from other laboratories, although results from other laboratories are mentioned at appropriate points.

Low-Temperature NMR to Study Temperature-Dependent Phenomena

Molecular Motions in Solid C_{60}. Since biological processes do not ordinarily occur at low temperatures, the phenomena that are studied by low-temperature NMR (and other low-temperature techniques) are generally drawn from the fields of physics, physical chemistry, and materials science. In physics, phenomena such as superconductivity,[1] antiferromagnetism,[2] and charge density waves[3] have been the subjects of numerous low-temperature NMR studies.

When simple methods for producing macroscopic quantities of the all-carbon molecules called fullerenes were invented in 1990,[4] my colleagues at AT&T Bell Laboratories and I investigated the dynamics of fullerenes in the solid state, originally with the idea that the soccer-ball shape proposed for the "buckminsterfullerene" C_{60} molecule might lead to isotropic molecular rotation within solid C_{60}. This idea was born out by the natural-abundance ^{13}C NMR spectra of C_{60} powder shown in Figure 1a, which show the broad chemical shift anisotropy (CSA) powder pattern line shape expected for static molecules at temperatures below 140 K, but a single line at the isotropic chemical shift position at higher temperatures.[5] The temperature-dependent change in the ^{13}C NMR spectrum is due to averaging of the CSA to zero at the higher temperatures by rapid molecular reorientiation, together with the fact that all carbon sites in C_{60} are related by rotational symmetry, making their isotropic chemical shifts equal.

On the other hand, diffraction measurements on C_{60} powder by Heiney et al.[6] seemed to show that molecular motion stopped at an orientational order–disorder phase transition at $T_c \approx 250$ K. More precisely, C_{60} molecules appeared as nearly featureless spheres in diffraction data above T_c, but as objects with the expected icosahedral symmetry below T_c. Yet the solid state NMR spectra in Figure 1a showed that rotational motion on the microsecond time scale continued down to 150 K.

The apparent contradiction between NMR and diffraction results for solid C_{60} was resolved by the temperature-dependent ^{13}C spin–lattice relaxation time (T_1) measurements shown in Figure 1b. These measurements show that the nature of molecular motions changes qualitatively at the phase transition identified by diffraction, from reorientation on the ~20 ps time scale immediately above T_c (which we found to be 260 K) to reorientation on the ~3 ns time scale immediately below T_c.[5] Above the phase transition, C_{60} molecules reorient by rotational diffusion, assuming all possible orientations with nearly equal probabilities and therefore appearing as spheres in diffraction data. Below the phase transition, C_{60} molecules reorient by thermally activated jumps among symmetry-related orientations and therefore appear as icosahedrally symmetry objects in diffraction data.

Skyrmions in Two-Dimensional Electron Systems. Technologically important devices often depend on thin-film materials, which are difficult to study by NMR due to the low sensitivity of conventional NMR measurements. For this reason, we became interested in optical pumping of nuclear spin polarizations in III–V semiconductors, a phenomenon in which excitation of electron–hole pairs by light tuned near the semiconductor band gap energy leads to the creation of large nuclear spin polarizations through hyperfine couplings between photoexcited electrons and nuclei.[7] Optical pumping can generate nuclear spin polarizations on the order of 10%,[8] but requires low temperatures where electron spin–lattice relaxation times (T_{1e}) and excited-state lifetimes are relatively long.

Our optical pumping experiments focused on GaAs/AlGaAs quantum well samples, that is, samples produced by molecular beam epitaxy in which thin GaAs layers were separated by thicker AlGaAs layers. Due to the lower band gap energy in GaAs than in AlGaAs, the GaAs layers act as potential energy wells for conduction electrons, confining the conduction electrons to states that are essentially two-dimensional (2D) at sufficiently low temperatures.[9]

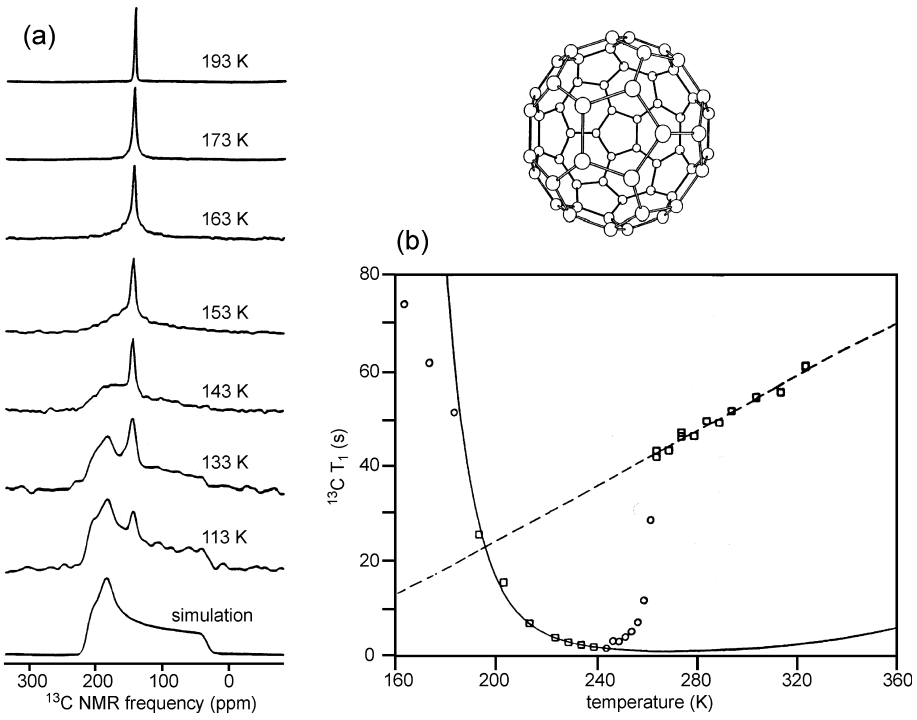

FIGURE 1. (a) ^{13}C NMR spectra of polycrystalline C_{60} at the indicated temperatures and 9.39 T, compared with the simulated chemical shift anisotropy powder pattern line shape for immobilized molecules. (b) Experimental temperature dependence of the spin–lattice relaxation time (squares and circles) and best-fit theoretical curves for low-temperature and high-temperature phases (solid and dashed lines, respectively) with different activation energies for molecular reorientation. Adapted with permission from ref 5. Copyright 1991 American Physical Society.

Strong optical pumping effects had already been demonstrated in GaAs,[10,11] interesting phenomena such as the integral and fractional quantum Hall effects were known to occur in GaAs/AlGaAs quantum wells,[12] and our Bell Laboratories colleagues Loren Pfeiffer and Ken West could fabricate high-quality samples. Although what we would learn from optically pumped NMR measurements on quantum wells was not entirely clear at the outset, the fact that similar measurements on similar samples had not been attempted before suggested that new information was likely to emerge from these experiments.

Figure 2a shows ^{71}Ga NMR spectra of a quantum well sample at 1.6 K after various optical pumping times.[13,14] At short times, the spectrum contains one relatively broad line, arising from the GaAs layers where optical pumping occurs. At longer times, a second, sharper line grows in due to ^{71}Ga–^{71}Ga spin diffusion that transports optically pumped nuclear spin polarization to the AlGaAs layers. The frequency shift K between GaAs and AlGaAs lines is due to contact hyperfine couplings between ^{71}Ga nuclei and electrons in the wells.

Figure 2b shows that *K* has a surprising dependence on a quantity called the Landau-level filling factor, or ν, which is the ratio between the *actual* number of electrons per unit area in a quantum well and the *maximum* number per unit area that can accommodated in a single state of transverse cyclotron motion (called a Landau level) with the same spin direction.[9] At $\nu = 1$, *K* has its maximum value, indicating that all 2D electrons are fully polarized (i.e., have the same spin direction). But as ν becomes either slightly greater than or slightly less than one, *K* drops rapidly, indicating that many electrons flip their spins when a single extra electron is added or subtracted from the 2D electron system. In effect, each extra electron carries a spin substantially greater than 1/2. These unusual electron states arise from electron–electron interactions within the 2D electron system, and are called "skyrmions". Data in Figure 2b constitute the first experimental evidence that skyrmions exist in 2D electron systems at low temperatures and in strong magnetic fields.[13,14] These data stimulated a wave of subsequent experimental and theoretical studies of skyrmions in the quantum well research community.[15–17]

Low-Temperature NMR to Immobilize Proteins

In studies of proteins and other biopolymers, multidimensional solution NMR measurements constitute a powerful approach to full structure determination and detailed

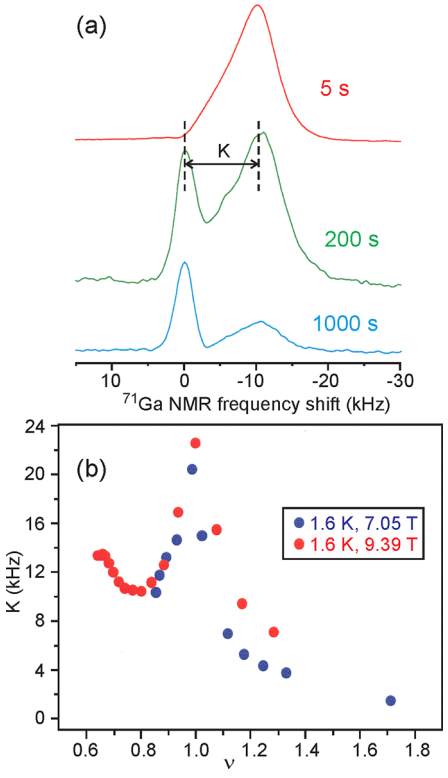

FIGURE 2. (a) ^{71}Ga NMR spectra of a GaAs/AlGaAs quantum well (40 n-doped GaAs layers, 30 nm thick, separated by 180 nm AlGaAs layers, ~0.3 cm^2 area) at 1.6 K and 7.05 T, with optical pumping at 806 nm wavelength for the indicated times after saturation of ^{71}Ga spin polarization. (b) Dependence of the hyperfine shift K between GaAs and AlGaAs signals on Landau-level filling factor ν, varied by tilting the sample relative to the external magnetic field, at 7.05 and 9.39 T.[13]

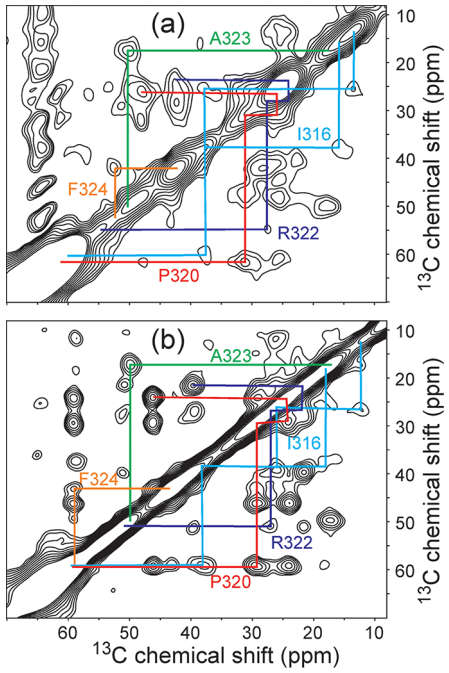

FIGURE 3. Aliphatic regions of 2D ^{13}C–^{13}C NMR spectra of a 20-residue peptide from the V3 loop of HIV-1 gp120 in the free (a) and antibody-bound (b) states, recorded in frozen solutions at 153 K and 9.39 T with MAS. Adapted with permission from ref 19. Copyright 2004 American Chemical Society. The peptide is uniformly ^{15}N,^{13}C-labeled in seven consecutive residues, including the five nonglycine residues whose crosspeak signals are indicated by color-coded assignment paths.

dynamical characterization of proteins and other biopolymers. However, these measurements become less informative as molecular weight increases and rotational diffusion slows down. In contrast, solid state NMR methods are applicable to biopolymers of arbitrarily high molecular weight, provided that some form of selective isotopic labeling is used, that natural-abundance ^{13}C signals are not overwhelming, and that sufficiently high concentrations can be achieved. Thus, even for soluble proteins, it can be advantageous to freeze the sample and apply solid state NMR methods.

Figure 3 shows one example, taken from our efforts to determine the conformations of peptides derived from the third variable (V3) loop of the HIV-1 gp120 protein when bound to anti-gp120 antibodies.[18,19] The V3 loop is of particular interest both because it is a primary target of antibodies that neutralize HIV-1 and because it interacts with chemokine receptors on host cell surfaces during the infection process. In Figure 3a, the 2D ^{13}C–^{13}C spectrum of a free V3 peptide, uniformly ^{15}N,^{13}C-labeled at seven successive residues, shows relatively broad crosspeak signals in frozen glycerol/water at 153 K under magic-angle spinning (MAS), indicating substantial conformational disorder. In Figure 3b, the 2D spectrum of the antibody-bound peptide shows much sharper signals, about 1.8 ppm wide (full width at half-maximum), indicating a well-defined conformation in the peptide/antibody complex. From ^{13}C chemical shifts and ^{13}C–^{13}C distance measurements, it was possible to develop a structural model for the epitope region of the antibody-bound V3 loop.[19]

Measurements in Figure 3 were performed at 9.39 T, with 6 mm diameter MAS rotors and a 240 μL sample volume. The sample was cooled with cold N_2 gas, supplied to the sample space within the MAS module from the top of the magnet. To reduce the ^{1}H T_1 value to ~1 s and thereby accelerate data acquisition, paramagnetic Cu^{2+} (20 mM $CuNa_2EDTA$) was added to the frozen solutions, as originally demonstrated by Weliky et al.[18] With a 1.0 mM peptide/antibody concentration, the 2D spectrum in Figure 3b was acquired in about 90 h.

Similar measurement conditions were used to acquire the data in Figure 4. In these experiments on the 35-residue villin headpiece subdomain (HP35), a popular model protein for

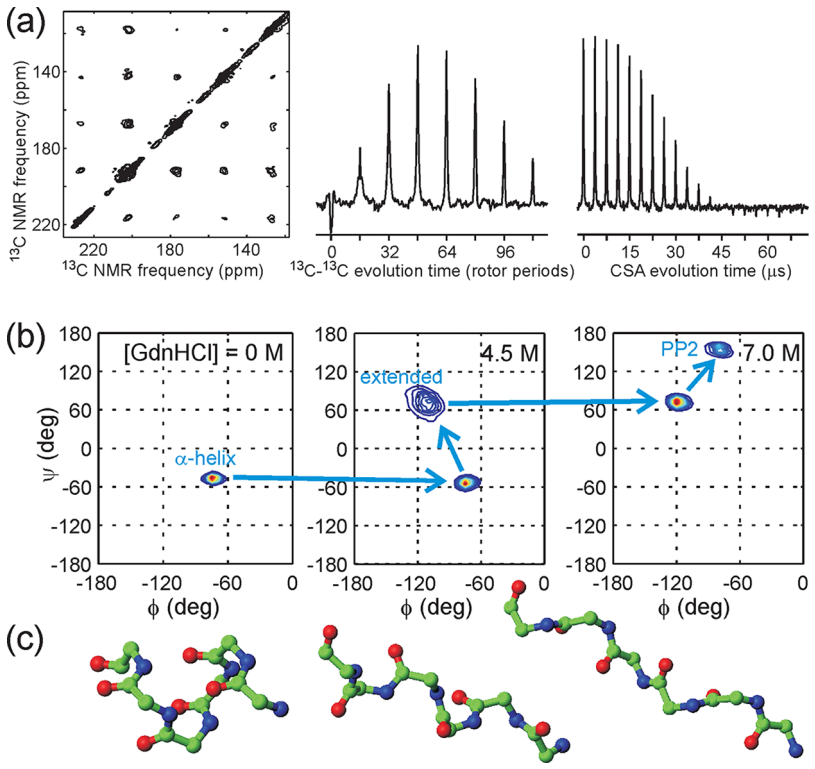

FIGURE 4. (a) 2D MAS exchange spectrum[25] (left), constant-time double-quantum-filtered dipolar evolution data[26] (center), and double-quantum CSA data[27] (right) for HP35 in glycerol/water at 153 K. Left panel: The protein is ^{13}C-labeled at carbonyl sites of A49 and V50; the data place constraints on the backbone ϕ and ψ angles of V50.[28] (b) Backbone conformational distributions at V50 for HP35 in frozen solution with indicated denaturant concentrations, derived from data as in panel (a). (c) Models of a polypeptide backbone with the α-helical, extended, and polyproline II (PP2) conformations that are predominant components of the distributions in panel (b).

folding studies,[20−23] we investigated the dependence of site-specific conformational distributions on the extent of unfolding induced by the denaturant guanidine hydrochloride (GdnHCl). In its fully folded state, HP35 is a three-helix bundle.[24] For solid state NMR measurements, HP35 samples were ^{13}C-labeled at sequential pairs of backbone carbonyl sites; quantitative structural techniques developed in my laboratory[25−27] were used to place constraints on the backbone ϕ and ψ torsion angles between the labeled sites. The solid state NMR data revealed the specific conformational pathway shown in Figure 4, in which helical segments present at [GdnHCl] = 0 convert first to mixtures of helical and extended conformations near the unfolding midpoint at [GdnHCl] = 4.5 M, then to mixtures of extended and polyproline II conformations in the fully unfolded state at [GdnHCl] = 7.0 M.[28] Identification of this conformational pathway was purely a consequence of the solid state NMR data, with no reliance on structural databases, prior expectations, or other measurements.

These experiments on HP35 show how detailed structural information about unfolded states of proteins can be obtained from solid state NMR, information that is difficult to obtain from other experimental techniques. These experiments also illustrate how low-temperature NMR can be used to suppress conformational exchange in unfolded states (in addition to rotational diffusion), allowing conformational distributions to be characterized at a quantitative and site-specific level.

Low-Temperature NMR to Trap Transient States

Partially and fully unfolded states created by addition of a chemical denaturant are equilibrium states. Transient, nonequilibrium states can also be created if solvent conditions, such as temperature, pH, ionic strength, or denaturant concentration, are changed rapidly from conditions that favor the unfolded state to conditions that favor the folded state. If a protein solution can be frozen on a time scale less than the structural equilibration time, then solid state NMR measurements can be used to characterize the protein structure in a transient intermediate state.

Figure 5 shows examples of data from our initial demonstration of solid state NMR as a structural probe of transient states in a nonequilibrium protein folding process.[29] In these

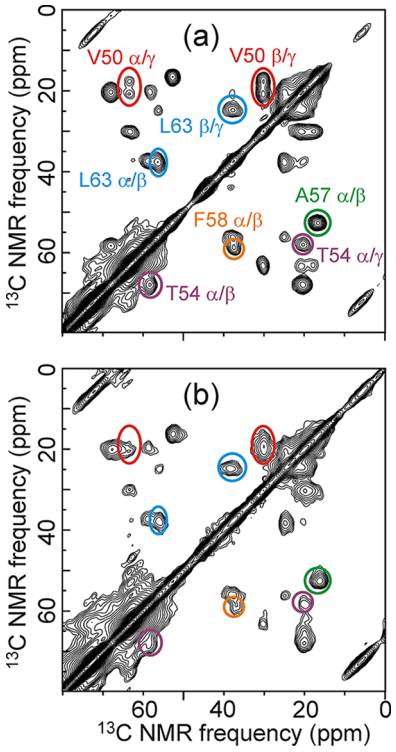

FIGURE 5. Aliphatic regions of 2D $^{13}C-^{13}C$ NMR spectra of HP35 in fully folded (a) and freeze-trapped intermediate (b) states, recorded in glycerol/water at 153 K and 9.39 T with MAS. Color-coded ellipses indicate crosspeak signals that are significantly shifted or broadened in the partially folded intermediate state, for the uniformly ^{13}C-labeled residues V50, T54, A57, F58, and L63.[29]

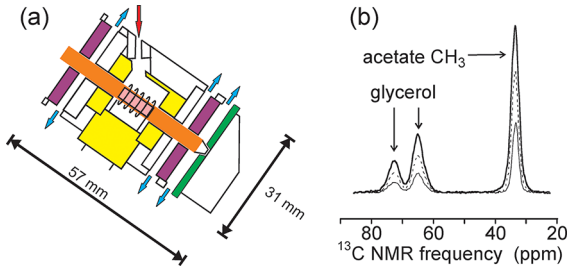

FIGURE 6. (a) Diagram of MAS module for ultralow-temperature solid state NMR experiments.[32] The rotor (orange) is supported by bearings (purple) and spun by a stator (green) that are driven by nitrogen gas, which exits as indicated by blue arrows. Cold helium (red arrow) enters the space around the rf coil and sample (pink) that is defined by the Teflon insert (yellow) and exits along the outer surface of the rotor, toward the bearings. (b) ^{13}C MAS spectra of $^{13}CH_3$-labeled sodium acetate in glycerol/water at 25 K (heavy solid line), 40 K (dashed line), and 79 K (thin solid line), recorded at 9.39 T with 7.00 kHz MAS.

experiments, a glycerol/water solution of HP35 was heated to 363 K, creating a thermally unfolded state, then frozen by spraying a fine jet of the solution into a bath of isopentane at 128 K. Under our conditions, the time to cool from above 80 to 0 °C was 10−20 μs. Comparison of 2D $^{13}C-^{13}C$ NMR spectra of HP35 solutions that were frozen slowly from room temperature (Figure 5a) with spectra of solutions that were frozen rapidly from 363 K (Figure 5b) showed that the 10−20 μs freeze-quenching time was sufficient to trap an intermediate state. Distributions of crosspeak intensity in the 2D spectra showed that this intermediate state has about 60% of the helical secondary structure but not the full tertiary structure (i.e., ordered packing of the hydrophobic core) of fully folded HP35. In fact, no fully folded HP35 molecules were detected in spectra of the freeze-quenched intermediate state. This result is particularly interesting because previous studies of HP35 folding by optical spectroscopy[20] and recent computational studies[23] suggest a time scale less than 5 μs for folding (although under somewhat different conditions).

Even with Cu^{2+} doping, a 200 μL sample volume, a 153 K sample temperature, and a 4 mM protein concentration, 2D spectra as in Figure 5b required 100−240 h of data acquisition. To make experiments of this sort more practical, further sensitivity enhancements are clearly needed.

Low-Temperature NMR to Enhance Sensitivity

Nuclear spin polarizations at thermal equilibrium are proportional to $1/T$, where T is the sample temperature. The noise amplitude from radio frequency (rf) circuitry in the NMR probe is proportional to $T^{-1/2}$, if all circuit elements are at temperature T. The quality factor (Q) of the rf circuit generally increases with decreasing temperature. Experiments in Figures 1 and 2 were performed without MAS, using cryostats in which samples were cooled with (Figure 1) or immersed in (Figure 2) liquid helium. Experiments in Figures 3−5 were performed with commercial MAS NMR probes, in which samples were cooled with cold nitrogen gas, resulting in only modest sensitivity enhancements from temperature reduction. Since the signal-to-noise ratio in an NMR spectrum, acquired with a given number of scans and a given sample size, is expected to increase by a factor of at least 15−60 when T is reduced from 300 to 20 K, and since most studies of biomolecular systems require MAS, it is clearly desirable to develop MAS NMR probes that operate at temperatures near 20 K, using liquid helium to cool the sample and perhaps the circuitry. MAS probe designs in which helium is used both to cool the sample and to supply gas to the MAS drive and bearing components suffer from high liquid helium consumption rates and relatively low MAS frequencies[30] unless MAS rotor volumes are small.[31] We therefore chose to pursue an ultralow-temperature MAS design in which nitrogen is used as the MAS drive and bearing gas, while helium is used only for sample cooling.

Figure 6a shows the MAS system.[32] We use zirconia MAS rotors with 4 mm outer diameter, 45.7 mm length, and a maximum sample volume of 82 μL. The low thermal conductivity of zirconia and the large rotor length allow the sample to be cooled to 20−25 K with helium, while the bearing and drive areas are well above 77 K. A Teflon insert within the MAS module limits the helium-cooled volume to a minimal space around the rf coil. Cold helium from a liquid helium transfer line enters the MAS module from above and exits the sample area by flowing toward the bearings through the narrow gap between the rotor sleeve and the Teflon insert. Vent holes near the bearings ensure that nitrogen bearing gas does not enter the helium-cooled volume. With this design, stable spinning at MAS frequencies up to 7.0 kHz is achieved with 20−25 K sample temperatures and liquid helium consumption rates of 2−4 l/h. Rf performance is quite comparable to conventional MAS NMR probes. Rf arcing is not a serious problem, even during measurements that involve cross-polarization and ^{1}H decoupling at high powers, provided that helium gas is not allowed to escape from the sample space along the leads of the rf coil.

Figure 6b shows ^{13}C MAS NMR spectra obtained at temperatures between 40 and 79 K, demonstrating the $1/T$ dependence of signal amplitudes on sample temperature.[32] In practice, only minor reductions in noise and increases in Q with decreasing temperature are observed, because only the rf coil (and not the rest of the rf circuitry) is cooled in our current probe design. Sample temperatures in Figure 6b were determined from measurements of the T_1 of ^{79}Br in KBr powder, which can be measured quickly in a probe that tunes near the ^{13}C NMR frequency and which decreases monotonically from 140 to 2.6 s in the temperature range from 20 to 60 K.[33] A less accurate, but nonetheless useful, assessment of sample temperature can be obtained from a fiber optic temperature sensor that is inserted into the helium-cooled volume within the MAS module.

^{1}H T_1 values for biomolecular samples near 20 K can be substantially greater than 10 s, especially for soluble, monomeric proteins in frozen glycerol/water solutions, where the effective ^{1}H T_1 is dominated by the T_1 of the solvent. Slow ^{1}H spin−lattice relaxation at low temperatures limits the rate at which data can be acquired, reducing the sensitivity advantage of low-temperature measurements. Near 20 K, the T_{1e} of Cu^{2+} becomes too long for Cu^{2+} to be an effective paramagnetic relaxation agent. As an alternative, we have found that Dy^{3+} in the form of DyH-EDTA at concentrations near 0.2 mM works well as a relaxation agent for monomeric proteins.[32] On the other hand, even without paramagnetic doping, certain macromolecular assemblies such as amyloid fibrils may exhibit ^{1}H T_1 values of approximately 5 s near 20 K, presumably due to a large local concentration of methyl groups (or perhaps other chemical groups) with motional correlation times in the nanosecond range.

Dynamic Nuclear Polarization at Ultralow Temperatures

Dynamic nuclear polarization is a phenomenon in which irradiation of electron paramagnetic resonance (EPR) transitions at microwave frequencies leads to enhancements of nuclear spin polarizations, and hence NMR signals, through cross-relaxation processes driven by electron−nucleus hyperfine couplings.[34,35] While my laboratory was developing the ultralow-temperature MAS probe design described above, the M.I.T. group led by R. G. Griffin began to obtain quite promising results from their efforts to apply dynamic nuclear polarization (DNP) to biomolecular solid state NMR with MAS at high magnetic fields.[36] Among their many contributions to DNP methods, the M.I.T. group showed that nitroxide radicals could be used as paramagnetic dopants in frozen solutions, leading to large enhancements of ^{1}H spin polarizations relative to thermal equilibrium values (i.e., DNP enhancement factors, ε_{DNP}) through the "cross effect" mechanism, especially when pairs of nitroxide moieties were combined within biradical dopants.[37,38] In addition, they showed that continuous-wave gyrotrons are effective sources of high-power microwaves at the EPR frequencies in high-field NMR magnets.[39]

DNP generally requires that electron spin polarizations be perturbed from thermal equilibrium (i.e., partially saturated) by the applied microwaves, implying that the microwave fields must be strong enough to produce electron spin Rabi frequencies comparable to electron spin−lattice relaxation rates ($1/T_{1e}$). DNP experiments with MAS at M.I.T. were performed at 80 K or higher temperatures, where T_{1e} values for nitroxides are 0.1−1 ms.[40,41] Since we had constructed a MAS NMR probe that could operate in the 20−25 K range, we decided to explore the possibility of performing DNP experiments at ultralow temperatures, where nitroxide T_{1e} values can be greater than 1 ms.[42,43] With longer T_{1e}, lower-power microwave sources could be used. In addition, intrinsic nuclear T_1 values (i.e., T_1 values in the absence of paramagnetic doping) are expected to be longer, at least in certain classes of samples, possibly leading to larger values of ε_{DNP} in cases where intrinsic nuclear spin−lattice relaxation competes with DNP processes. Finally, since ε_{DNP} represents

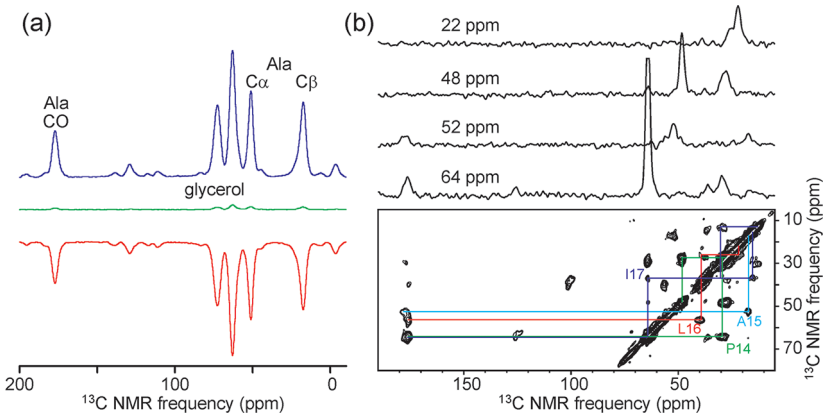

FIGURE 7. (a) ^{13}C NMR spectra of 50 mM uniformly ^{13}C-labeled L-alanine in partially deuterated glycerol/water with 10 mM DOTOPA-TEMPO, recorded at 20 K and 9.39 T with 6.7 kHz MAS. Spectra are shown with 30 mW microwave irradiation at 264.05 GHz (blue) and 264.65 GHz (red), and without microwave irradiation (green). (b) 2D ^{13}C−^{13}C spectrum of the 26-residue peptide melittin in partially deuterated glycerol/water with 9.9 mM DOTOPA-TEMPO, recorded at 25 K and 9.39 T with 6.4 kHz MAS. 1D slices at indicated positions are shown above the 2D spectrum. The peptide is uniformly ^{13}C-labeled at P14, A15, L16, and I17. The peptide concentration is 1.9 mM, the sample volume is 82 μL, the recycle delay is 10 s, and the total measurement time is 2.2 h.[45]

the polarization enhancement relative to thermal equilibrium, a given value of ε_{DNP} corresponds to absolute polarizations at 20−25 K than at 80−100 K.

Our initial DNP experiments were performed without MAS, at 9.39 T and temperatures in the 7−80 K range, using a tunable microwave source with a 30 mW maximum output.[43] Measurements on frozen glycerol/water solutions of various nitroxide compounds yielded values of ε_{DNP} for ^{1}H spins as large as 80 at 7 K. The largest values of ε_{DNP} and shortest DNP build-up times (T_{DNP}) were obtained with a triradical compound, called DOTOPA-TEMPO.[43] In our hands, the absolute DNP-enhanced ^{1}H NMR sensitivity at 20 K with 30 mW microwave power was comparable to the absolute sensitivity expected hypothetically at 80 K with $\varepsilon_{DNP} \approx 130$ and $T_{DNP} \approx 1.4$ s. Similar enhancements of cross-polarized ^{13}C NMR sensitivity were observed in double-resonance DNP experiments at ultralow temperatures.[44] These results encouraged us to construct a version of the ultralow-temperature MAS probe that includes provisions for microwave irradiation for DNP.

Figure 7 shows ^{13}C MAS NMR spectra obtained recently with DNP at temperatures in the 20−25 K range, again at 9.39 T with a 30 mW microwave source.[45] One-dimensional spectra of $^{13}C_3$-L-alanine, dissolved in glycerol/water and doped with DOTOPA-TEMPO, show $\varepsilon_{DNP} \approx \pm 25$ at 20 K (Figure 7a). As predicted by theory and numerical calculations of cross-effect DNP under MAS,[46] the sign of the DNP-enhanced signal depends on the microwave frequency. The 2D ^{13}C−^{13}C spectrum of a model peptide (Figure 7b) shows that high-quality 2D data can be obtained in about 2 h from 82 μL of isotopically labeled peptides or proteins at 1.9 mM concentration.[45] Compared with the experimental conditions in Figure 5, this represents a 6-fold reduction in the quantity of labeled sample and a 50-to-120-fold reduction in the measurement time, constituting a net sensitivity enhancement factor in the 42−66 range.

Concluding Remarks

Experimental examples discussed above illustrate some of the important motivations for pursuing NMR measurements at low and ultralow temperatures, some of the techniques and technology that are associated with low-temperature experiments, and some of the likely directions for future research. In my laboratory, we are currently planning to apply ultralow-temperature DNP with MAS to several structural problems in biomolecular systems, including freeze-trapped intermediate states in protein folding and peptide aggregation processes and membrane-associated peptide/protein complexes. The success of these specific efforts may depend on factors that are now under investigation, such as intrinsic ^{1}H T_1 values and ^{13}C NMR linewidths under ultralow-temperature DNP conditions. Further optimization of paramagnetic dopants and other aspects of sample preparation may be required. Modifications of our DNP apparatus to increase the available microwave power and to reach lower sample temperatures while reducing liquid helium consumption are also in progress. Through this combination of exploratory applications to biomolecular systems and ongoing technological developments, it seems likely that ultralow-temperature NMR measurements will soon make

important contributions to our understanding of systems that are of widespread interest outside the community of solid state NMR spectroscopists.

Work described in this Account was supported by the Intramural Research Program of the National Institute of Diabetes and Digestive and Kidney Diseases, National Institutes of Health, and by the NIH Intramural AIDS Targeted Antiviral Program. I thank current and past members of my laboratory for their many contributions to this work. Data shown in the figures were acquired by Gary Dabbagh, Sean Barrett, Simon Sharpe, Kan-Nian Hu, and Kent Thurber.

BIOGRAPHICAL INFORMATION

Robert Tycko is a Senior Investigator in the NIH Intramural Research Program, where he has been since 1994. His educational background includes A.B. and Ph.D. degrees in chemistry, and 8 years as a Member of Technical Staff at AT&T Bell Laboratories. His research centers on solid state NMR and its applications in biophysics and biophysical chemistry.

FOOTNOTES

*Mailing address: National Institutes of Health, Building 5, Room 112, Bethesda, MD 20892-0520. Phone: 301-402-8272. Fax: 301-496-0825. E-mail: robertty@mail.nih.gov.

The authors declare no competing financial interest.

REFERENCES

1 Hebel, L. C.; Slichter, C. P. Nuclear Spin Relaxation in Normal and Superconducting Aluminum. *Phys. Rev.* **1959**, *113*, 1504–1519.

2 Jaccarino, V.; Shulman, R. G. Observation of Nuclear Magnetic Resonance in Antiferromagnetic $Mn^{19}F_2$. *Phys. Rev.* **1957**, *107*, 1196–1197.

3 Kramer, S.; Mehring, M. Low-Temperature Charge Ordering in the Superconducting State of $YBa_2Cu_3O_{7-\delta}$. *Phys. Rev. Lett.* **1999**, *83*, 396–399.

4 Kratschmer, W.; Lamb, L. D.; Fostiropoulos, K.; Huffman, D. R. Solid C_{60}: A New Form of Carbon. *Nature* **1990**, *347*, 354–358.

5 Tycko, R.; Dabbagh, G.; Fleming, R. M.; Haddon, R. C.; Makhija, A. V.; Zahurak, S. M. Molecular Dynamics and the Phase Transition in Solid C_{60}. *Phys. Rev. Lett.* **1991**, *67*, 1886–1889.

6 Heiney, P. A.; Fischer, J. E.; McGhie, A. R.; Romanow, W. J.; Denenstein, A. M.; McCauley, J. P.; Smith, A. B.; Cox, D. E. Orientational Ordering Transition in Solid C_{60}. *Phys. Rev. Lett.* **1991**, *66*, 2911–2914.

7 Lampel, G. Nuclear Dynamic Polarization by Optical Electronic Saturation and Optical Pumping in Semiconductors. *Phys. Rev. Lett.* **1968**, *20*, 491–493.

8 Michal, C. A.; Tycko, R.; Stray-Field, N. M. R. Imaging and Wavelength Dependence of Optically Pumped Nuclear Spin Polarization in InP. *Phys. Rev. B* **1999**, *60*, 8672–8679.

9 Weisbuch, C.; Vinter, B. *Quantum Semiconductor Structures: Fundamentals and Applications*; Academic Press: New York, 1991.

10 Paget, D. Optical Detection of NMR in High-Purity GaAs under Optical-Pumping: Efficient Spin-Exchange Averaging between Electronic States. *Phys. Rev. B* **1981**, *24*, 3776–3793.

11 Buratto, S. K.; Shykind, D. N.; Weitekamp, D. P. Time-Sequenced Optical Nuclear Magnetic Resonance of Gallium Arsenide. *Phys. Rev. B* **1991**, *44*, 9035–9038.

12 Willett, R.; Eisenstein, J. P.; Stormer, H. L.; Tsui, D. C.; Gossard, A. C.; English, J. H. Observation of an Even-Denominator Quantum Number in the Fractional Quantum Hall Effect. *Phys. Rev. Lett.* **1987**, *59*, 1776–1779.

13 Barrett, S. E.; Dabbagh, G.; Pfeiffer, L. N.; West, K. W.; Tycko, R. Optically Pumped Nmr Evidence for Finite-Size Skyrmions in GaAs Quantum Wells near Landau-Level Filling $\nu = 1$. *Phys. Rev. Lett.* **1995**, *74*, 5112–5115.

14 Tycko, R.; Barrett, S. E.; Dabbagh, G.; Pfeiffer, L. N.; West, K. W. Electronic States in Gallium Arsenide Quantum Wells Probed by Optically Pumped NMR. *Science* **1995**, *268*, 1460–1463.

15 Aifer, E. H.; Goldberg, B. B.; Broido, D. A. Evidence of Skyrmion Excitations About ν=1 in n-Modulation-Doped Single Quantum Wells by Interband Optical Transmission. *Phys. Rev. Lett.* **1996**, *76*, 680–683.

16 Bayot, V.; Grivei, E.; Melinte, S.; Santos, M. B.; Shayegan, M. Giant Low Temperature Heat Capacity of GaAs Quantum Wells near Landau Level Filling $\nu = 1$. *Phys. Rev. Lett.* **1996**, *76*, 4584–4587.

17 Fertig, H. A.; Brey, L.; Cote, R.; MacDonald, A. H.; Karlhede, A.; Sondhi, S. L. Hartree-Fock Theory of Skyrmions in Quantum Hall Ferromagnets. *Phys. Rev. B* **1997**, *55*, 10671–10680.

18 Weliky, D. P.; Bennett, A. E.; Zvi, A.; Anglister, J.; Steinbach, P. J.; Tycko, R. Solid State NMR Evidence for an Antibody-Dependent Conformation of the V3 Loop of HIV-1 gp120. *Nat. Struct. Biol.* **1999**, *6*, 141–145.

19 Sharpe, S.; Kessler, N.; Anglister, J. A.; Yau, W. M.; Tycko, R. Solid State NMR Yields Structural Constraints on the V3 Loop from HIV-1 gp120 Bound to the 447−52d Antibody Fv Fragment. *J. Am. Chem. Soc.* **2004**, *126*, 4979–4990.

20 Kubelka, J.; Eaton, W. A.; Hofrichter, J. Experimental Tests of Villin Subdomain Folding Simulations. *J. Mol. Biol.* **2003**, *329*, 625–630.

21 Wang, M. H.; Tang, Y. F.; Sato, S. S.; Vugmeyster, L.; McKnight, C. J.; Raleigh, D. P. Dynamic NMR Line Shape Analysis Demonstrates that the Villin Headpiece Subdomain Folds on the Microsecond Time Scale. *J. Am. Chem. Soc.* **2003**, *125*, 6032–6033.

22 Freddolino, P. L.; Schulten, K. Common Structural Transitions in Explicit-Solvent Simulations of Villin Headpiece Folding. *Biophys. J.* **2009**, *97*, 2338–2347.

23 Piana, S.; Lindorff-Larsen, K.; Shaw, D. E. Protein Folding Kinetics and Thermodynamics from Atomistic Simulation. *Proc. Natl. Acad. Sci. U.S.A.* **2012**, *109*, 17845–17850.

24 McKnight, C. J.; Matsudaira, P. T.; Kim, P. S. NMR Structure of the 35-Residue Villin Headpiece Subdomain. *Nat. Struct. Biol.* **1997**, *4*, 180–184.

25 Weliky, D. P.; Tycko, R. Determination of Peptide Conformations by Two-Dimensional Magic Angle Spinning NMR Exchange Spectroscopy with Rotor Synchronization. *J. Am. Chem. Soc.* **1996**, *118*, 8487–8488.

26 Bennett, A. E.; Weliky, D. P.; Tycko, R. Quantitative Conformational Measurements in Solid State NMR by Constant-Time Homonuclear Dipolar Recoupling. *J. Am. Chem. Soc.* **1998**, *120*, 4897–4898.

27 Blanco, F. J.; Tycko, R. Determination of Polypeptide Backbone Dihedral Angles in Solid State NMR by Double Quantum ^{13}C Chemical Shift Anisotropy Measurements. *J. Magn. Reson.* **2001**, *149*, 131–138.

28 Hu, K. N.; Havlin, R. H.; Yau, W. M.; Tycko, R. Quantitative Determination of Site-Specific Conformational Distributions in an Unfolded Protein by Solid State Nuclear Magnetic Resonance. *J. Mol. Biol.* **2009**, *392*, 1055–1073.

29 Hu, K. N.; Yau, W. M.; Tycko, R. Detection of a Transient Intermediate in a Rapid Protein Folding Process by Solid State Nuclear Magnetic Resonance. *J. Am. Chem. Soc.* **2010**, *132*, 24–25.

30 Hackmann, A.; Seidel, H.; Kendrick, R. D.; Myhre, P. C.; Yannoni, C. S. Magic-Angle Spinning NMR at Near-Liquid-Helium Temperatures. *J. Magn. Reson.* **1988**, *79*, 148–153.

31 Carravetta, M.; Johannessen, O. G.; Levitt, M. H.; Heinmaa, I.; Stern, R.; Samoson, A.; Horsewill, A. J.; Murata, Y.; Komatsu, K. Cryogenic NMR Spectroscopy of Endohedral Hydrogen-Fullerene Complexes. *J. Chem. Phys.* **2006**, *124*, 104507.

32 Thurber, K. R.; Tycko, R. Biomolecular Solid State NMR with Magic-Angle Spinning at 25 K. *J. Magn. Reson.* **2008**, *195*, 179–186.

33 Thurber, K. R.; Tycko, R. Measurement of Sample Temperatures under Magic-Angle Spinning from the Chemical Shift and Spin-Lattice Relaxation Rate of ^{79}Br in KBr Powder. *J. Magn. Reson.* **2009**, *196*, 84–87.

34 Carver, T. R.; Slichter, C. P. Polarization of Nuclear Spins in Metals. *Phys. Rev.* **1953**, *92*, 212–213.

35 Overhauser, A. W. Polarization of Nuclei in Metals. *Phys. Rev.* **1953**, *91*, 476–476.

36 Maly, T.; Debelouchina, G. T.; Bajaj, V. S.; Hu, K. N.; Joo, C. G.; Mak-Jurkauskas, M. L.; Sirigiri, J. R.; van der Wel, P. C. A.; Herzfeld, J.; Temkin, R. J.; Griffin, R. G. Dynamic Nuclear Polarization at High Magnetic Fields. *J. Chem. Phys.* **2008**, *128*, 052201.

37 Hu, K. N.; Yu, H. H.; Swager, T. M.; Griffin, R. G. Dynamic Nuclear Polarization with Biradicals. *J. Am. Chem. Soc.* **2004**, *126*, 10844–10845.

38 Hu, K. N.; Debelouchina, G. T.; Smith, A. A.; Griffin, R. G. Quantum Mechanical Theory of Dynamic Nuclear Polarization in Solid Dielectrics. *J. Chem. Phys.* **2011**, 134.

39 Bajaj, V. S.; Farrar, C. T.; Hornstein, M. K.; Mastovsky, I.; Vieregg, J.; Bryant, J.; Elena, B.; Kreischer, K. E.; Temkin, R. J.; Griffin, R. G. Dynamic Nuclear Polarization at 9 T Using a Novel 250 GHz Gyrotron Microwave Source. *J. Magn. Reson.* **2003**, *160*, 85–90.

40 Sato, H.; Kathirvelu, V.; Spagnol, G.; Rajca, S.; Rajca, A.; Eaton, S. S.; Eaton, G. R. Impact of Electron-Electron Spin Interaction on Electron Spin Relaxation of Nitroxide Diradicals and Tetraradicals in Glassy Solvents between 10 and 300 K. *J. Phys. Chem. B* **2008**, *112*, 2818–2828.

41 Zagdoun, A.; Casano, G.; Ouari, O.; Lapadula, G.; Rossini, A. J.; Lelli, M.; Baffert, M.; Gajan, D.; Veyre, L.; Maas, W. E.; Rosay, M.; Weber, R. T.; Thieuleux, C.; Coperet, C.; Lesage, A.;

Tordo, P.; Emsley, L. A Slowly Relaxing Rigid Biradical for Efficient Dynamic Nuclear Polarization Surface-Enhanced NMR Spectroscopy: Expeditious Characterization of Functional Group Manipulation in Hybrid Materials. *J. Am. Chem. Soc.* **2012**, *134*, 2284–2291.

42 Farrar, C. T.; Hall, D. A.; Gerfen, G. J.; Inati, S. J.; Griffin, R. G. Mechanism of Dynamic Nuclear Polarization in High Magnetic Fields. *J. Chem. Phys.* **2001**, *114*, 4922–4933.

43 Thurber, K. R.; Yau, W. M.; Tycko, R. Low-Temperature Dynamic Nuclear Polarization at 9.4 T with a 30 mW Microwave Source. *J. Magn. Reson.* **2010**, *204*, 303–313.

44 Potapov, A.; Thurber, K. R.; Yau, W. M.; Tycko, R. Dynamic Nuclear Polarization-Enhanced ^{1}H-^{13}C Double Resonance NMR in Static Samples Below 20 K. *J. Magn. Reson.* **2012**, *221*, 32–40.

45 Thurber, K. R.; Potapov, A.; Yau, W. M.; Tycko, R. Solid State Nuclear Magnetic Resonance with Magic-Angle Spinning and Dynamic Nuclear Polarization Below 25 K. *J. Magn. Reson.* **2013**, *226*, 100–106.

46 Thurber, K. R.; Tycko, R. Theory for Cross Effect Dynamic Nuclear Polarization under Magic-Angle Spinning in Solid State Nuclear Magnetic Resonance: The Importance of Level Crossings. *J. Chem. Phys.* **2012**, 137.